Acta Radiologica

Dual Energy CT Imaging of Atherosclerotic Plaque using Novel Ultrasmall Superparamagnetic Iron Oxide in Hyperlipidemic Rabbits

Journal:	*Acta Radiologica*
Manuscript ID	Draft
Manuscript Type:	Original Article
Keywords:	dual energy computed tomography,, ultra-small superparamagnetic iron oxide, atherosclerotic plaque imaging, macrophage, iron-based map

Abstract

Background: A study using MRI revealed that ultra-small superparamagnetic iron oxide is phagocytosed by macrophages. However, MRI has limitations to obtain clear images due to its poor spatial and temporal resolutions.

Purpose: To examine whether the use of dual energy CT (DECT) facilitated the visualization of carboxymethyl-diethylaminoethyl dextran magnetite ultra-small superparamagnetic iron oxide (CMEADM-U) accumulation in arteriosclerotic lesions using hyperlipidemic rabbits.

Material & Methods: CMEADM-U at 0.5 mmol Fe/kg was administered to Watanabe hereditary atherosclerotic (WHHL) rabbits (n=6, 24 sections) and New Zealand white (NZW) rabbits (n=2, 6 sections). After 72 hours, DECT was performed to prepare virtual monochromatic images (VMI: 35keV, 70keV) and an iron-based map. Subsequently, the aorta was collected, and hematoxylin & eosin staining, berlin blue staining, and RAM11 immunostaining.

Results: In the WHHL rabbits, CMEADM-U accumulation was not observed at 70 keV. However, CMEADM-U accumulation consistent with an arteriosclerotic lesion was observed at 35 keV and the iron-based map. On the other hand, in the NZW rabbits, there was no CMEADM-U accumulation in any images. Further, there were significant differences in the iron-based map value at the site of accumulation among the grades of expression on berlin blue staining and RAM11 immunostaining. In addition, there was a good correlation at 35kev and iron-based map value ($r=0.42$, $p<0.05$).

Conclusion: DECT imaging for CMEADM-U facilitated the assessment of macrophage accumulation in atherosclerotic lesions in an *in vivo* study using a rabbit model of induced aortic atherosclerosis.

Key words

dual energy computed tomography, ultra-small superparamagnetic iron oxide, atherosclerotic plaque imaging, macrophage, iron-based map

Introduction

Acute coronary syndrome is caused by the plaque rupture around the coronary artery wall in approximately two-thirds of patients. As characteristics of plaque that is prone to rupture, a thin, fibrous capsule (<65 μm), positive remodeling, and a present of abundant of oxidized low-density lipoprotein cholesterol and macrophages were reported (1-3). In particular, the accumulation of macrophages caused by inflammation may play an important role in plaque destabilization, but no molecular imaging method to evaluate coronary plaque inflammation has been established. Ultra-small superparamagnetic iron oxide (USPIO) was developed as contrast medium for magnetic resonance imaging (MRI). The particle diameter is markedly small, approximately 50 nm and its blood retention time is long. As USPIO is phagocytosed by macrophages, previous studies using magnetic resonance angiography confirmed the macrophage accumulation of USPIO in arteriosclerotic lesions (4-5). Carboxymethyl-diethylaminoethyl dextran magnetite USPIO (CMEADM-U) was recently developed (6) as a new type, which accumulates in arteriosclerotic plaque macrophages more markedly and retains for a longer time than conventional USPIO. However, quantitative assessment using MRI is difficult in the analysis of small objects, such as coronary plaque, due to its poor spatial and temporal resolutions. Recently, dual-energy computed tomography (DECT), which is performed with two different energies, has become available. DECT scans can provide various images from two datasets which is proposed by the utilization of the attenuation coefficient, density, and CT values. Virtual monochromatic imaging (VMI), in which the effective energy can be randomly modified after imaging, can create images from those at lower than 70 keV corresponding to 120 kVp, which is primarily used on single-energy CT (SECT), and enhance the contrast (7). Furthermore, material density images obtained using 2- or 3-material decomposition methods can be visualized based on any substance; substances with similar CT values that cannot be visualized on SECT can be differentiated (8). A study previously reported that DECT images facilitated the visualization and even quantitative assessment of this novel USPIO using a phantom atherosclerotic model (9). However, its usefulness *in vivo* remains to be clarified. In this study, we administered CMEADM-U to a rabbit model for familial hypercholesterolemia and examined

whether DECT facilitates the visualization of arteriosclerotic plaque macrophage accumulation.

Material and methods

Study design

The study was approved by the governmental animal protection committee and the institutional review board for the care of animal subjects. All protocols were approved by the Intervention Technical Center Animal Welfare Committee (IVT-20-66) and experiments were conducted in accordance with the Animal Experiment Welfare Regulations. Our study is reported in accordance with ARRIVE guidelines.

Animal model and experimental protocol

As an atherosclerotic model, 4 Watanabe hereditary atherosclerotic (WHHL) rabbits (age: 10 months, mean body weight: 3.2 kg) were used. As a control model, 2 New Zealand white (NZW) rabbits (age: 10 months, mean body weight: 3.9 kg) were used. CMEADM-U at 0.5 mmol Fe/kg was administered 72 hours before CT imaging. The rabbits inhaled isoflurane through a mask and CT was performed under deep anesthesia. Subsequently, after confirming systemic collapse and analgesia under anesthesia control with isoflurane, an axillary incision was made and all animals were exsanguinated through the axillary artery. They were regarded as being euthanized by confirming an SpO_2 reaching zero on a bedside monitor and dilation of the pupils. Subsequently, the aorta was collected and fixed in paraformaldehyde. Paraffin blocks were prepared, and hematoxylin & eosin (HE) staining and Berlin blue staining (BB) were conducted using 3-μm-thick axial sections. Furthermore, specimens for immunostaining of macrophages (Macrophage clone RAM11: RAM11) were prepared using 4-μm-thick sections. The association with CMEADM-U accumulation was evaluated. Six sections per animal (total: 24 sections) from the WHHL rabbits and 3 (total: 6 sections) from the NZW rabbits were prepared. For alignment between CT images and pathological slices, the upper margin of the aortic arch and abdominal aorta-common iliac artery bifurcation were used as landmark.

CT protocol and CT analysis

All rabbits were scanned using Aquilion One PRISM Edition (Canon Medical Systems Corporation, Otawara, Japan). This system facilitates rapid kVp switching-type dual-energy scans (135 kVp and 80 kVp). The following imaging conditions were adopted: tube voltage, 135 and 80 kVp; tubal current, 100 and 570 mA; slice thickness, 0.5 mm; tube rotation speed, 0.5 s; rearrangement FOV, 240 mm; and matrix, 512 x 512. For image analysis, Vitrea workstation (Canon Medical Systems Corporation, Otawara, Japan) was used, and a DE-analyzing application, spectral analysis, were adopted. On VMI, image contrasts can be regulated by changing the effective energy. In this study, 35 keV, at which the highest contrast can be obtained, was used. Furthermore, images at 70 keV corresponding to 120 kVp, which is primarily used in clinical practice, were rearranged and compared. In addition, USPIO imaging at different concentrations was conducted, and an iron-based map with the 3-material-decomposition method was prepared by measuring the CT value for each concentration at 85 and 65 keV. For image measurement, the region of interest (ROI) for the vascular wall on each image was established. The CT value (Hounsfiedl unit; HU) was measured from VMI findings and the iron-based map value was from an iron-based map.

Histopathological examination

In the WHHL sections, the grade of accumulation on Berlin blue staining and RAM11 immunostaining was evaluated in 5 grades (grade 0: no accumulation, grade 1: ≤1/4 of the inner circumference of the aorta, grade 2: 1/4 to 2/4 of the inner circumference of the aorta, grade 3: 2/4 to 3/4 of the inner circumference of the aorta, and grade 4: entire inner circumference of the aorta) using a BHS binocular microscope (Olympus Corporation, Japan). The results were compared with those of DECT. In addition, for quantitative pathological analysis, virtual slides of the specimens (Aperio ImageScope, SVS mode) were prepared and screen shots of 2.0X zoom images were stored in TIFF format. On the TIFF images, the RAM11-positive area (μm^2) was measured using ImageJ (National Institute of Health, U.S.A.) and compared with the results of DECT. The image size was 1,284 x 692 pixels.

Statistical analysis

The data are expressed as the mean±standard deviation. To compare significant differences between two groups, the Student's t-test was used. For comparison among ≥3 groups, the analysis of variance (ANOVA) was adopted. For inter-group comparison, the Tukey honestly significant difference test was used. To examine the correlation between the RAM11-positive area obtained on quantitative pathological analysis and DECT, Pearson's correlation coefficient was used. A p-value of 0.05 was regarded as significant. Statistical analyses were performed using IBM SPSS ver23 software (IBM Institute Inc., U.S.A.).

Results

Pathological findings showed that atherosclerosis was not observed on HE staining (Fig 1a) in the control group, and the immunostaining was negative for either Berlin blue (Fig 1b) or RAM11 (Fig 1c). Contrary, in the atherosclerotic group, all slices exhibited atherosclerosis on HE staining (Fig 2a). The immunostaining was positive for Berlin blue (Fig 2b) staining and RAM11 (Fig 2c). In the control group, there was no accumulation on any DECT image of the same site as pathological sections (Fig 1; d, e, f). In the atherosclerotic group, CMEADM-U accumulation was not observed at 70 keV of VMI (Fig 2d), but contrast enhancement was obtained in the vascular wall at 35 keV (Fig 2e), where we identified the iron accumulation at an iron-based map (Fig 2f).

In the 24 sections in the atherosclerotic group, intimal hemosiderin deposition was assessed on Berlin blue staining. The grade was evaluated as 1 in 20 sections and 2 in 4. There was no grade -0, -3, or -4 sections (Table 1). When comparing the classification on Berlin blue stanning with the results of DECT, there was no significant difference between the grade-1 sections at 70 keV (37.86 ± 18.29 HU) and the grade-2 sections (39.98± 12.78 HU, $p = 0.82$) (Fig 3a). At 35 keV, there was no significant difference between the grade-1 sections (41.87 ± 55.35 HU) and the grade-2 sections (89.20 ± 43.12 HU, $p = 0.12$) (Fig 3b). However, using an iron-based map, significant differences were observed between the grade-1 sections (9.54 ± 9.47 HU) and the grade-2 sections (19.58 ± 3.87 HU, $p < 0.05$) (Fig 3c). Further, positive areas of macrophage were assessed on RAM11 immunostaining, the grade was evaluated as 2 in

5 sections, 3 in 8, and 4 in 11. There were no grade-0 or -1 sections (Table 1). When comparing positive-area classification on RAM11 immunostaining with the results of DECT, there were no significant difference between the grade-2 sections at 70 keV (33.34 ± 15.28 HU), the grade-3 sections (35.49 ± 21.80 HU), and the grade-4 sections (42.41 ± 14.93 HU, p = 0.56) (Fig 4a). However, using a 35keV, significant differences were observed between the grade-2 sections (17.78 ± 35.25 HU), the grade-3 sections (22.51 ± 62.24 HU), and the grade-4 sections (84.10 ± 38.91 HU. p< 0.05) (Fig 4b). When comparing the results between two groups, there were significant differences between the grade-2 sections and grade-4 sections (P < 0.05), and between the grade-3 sections and the grade-4 sections (P < 0.05) (Fig 4c). On the iron-based map, significant differences were observed between the grade-2 sections (4.65 ± 5.85), the grade-3 sections (6.78 ± 9.33), and the grade-4 sections (17.42 ± 7.37. P < 0.05). When comparing the results between two groups, there were significant differences between the grade-2 sections and grade-4 sections (p < 0.05), and between the grade-3 and grade-4 sections (P < 0.05).

Comparing the RAM11-positive area with the results of DECT, at 70 keV corresponding to conventional CT images, there was no correlation (r = 0.19) (Fig 5a). However, the RAM11-positive area was correlated with DECT images at 35 keV (r = 0.42, p < 0.05) (Fig 5b) and the iron-based map (r = 0.42, p < 0.05) (Fig 5c).

Discussion

To our knowledge, this is the first study in CMEADM-U accumulation was visualized at the site of atherosclerotic consistent with intimal hemosiderosis on Berlin blue staining and macrophage RAM11-positive reactions by performing DECT in an *in vivo* study. Previous studies also reported that USPIO facilitated the visualization of macrophage accumulation in the presence of atherosclerotic using MRI (4-5). However, the clinical application of MRI for the coronary artery was considered difficult due to its poor spatial/temporal resolutions and negative contrast medium. We hypothesized that the accumulation can be visualized using CT, which is clinically applicable for the coronary artery based on spatial/temporal resolutions. Indeed, contrast enhancement that was not expressed at 70 keV, corresponding to an energy zone on conventional SECT,

was obtained by performing DECT and adopting VMI at 35 keV. This result supports our previous study in which contrast enhancement effects were noted through the visualization of a low-energy area using DECT in a phantom experiment (9). Furthermore, when comparing CT findings with the pathological results, there was a significant difference in the CT value at the site of accumulation between the grades of RAM11-positive macrophages, but there was no significant difference in the grade of hemosiderosis on Berlin blue staining. Therefore, we utilized the 3-material decomposition method for DECT and prepared an iron-based map as the main component of CMEADM-U. In the 3-material decomposition method, iron-based map can be visualized from different concentrations (2.5 and 50 mg Fe/mL.) of CMEADM-U on DECT, which were based on the CT values at 65 and 85 keV in this study. As a result, there was a significant difference in the grade of hemosiderosis on Berlin blue staining and a high correlation with the RAM11-positive area. The quantitative assessment of macrophage accumulation, which reflects inflammation related to arteriosclerotic lesions, was also available.

A long blood retention time is important for USPIO to be sufficiently phagocytosed by intra-plaque macrophages. In this study, imaging was conducted 72 hours after administration based on the previous report (Stefan et al.), which indicated the difference in the signal to noise ratio (SNR) 72 hours after USPIO administration in an animal experiment using rabbits (10). As the blood retention time of CMEADM-U (6) is longer than that of conventional USPIO, the optimal timing of imaging may not be 72 hours after administration. However, in this study, serial imaging was not performed. As the half-life of USPIO in blood differs between humans and animals, the optimal timing of imaging for clinical application in humans must be further investigated. Concerning the dose, previous studies examined administration to animals at 1.0 mmol Fe/kg (10-11). This volume is larger than that previously administered to humans (12). However, due to differences in the half-life in blood, 0.2 to 1.0 mmol Fe/kg must be administered to animals when comparing it with 45 μmol/kg in humans (13). As the particle diameter of CMEADM-U is smaller than that of conventional USPIO, a dose of 0.5 mmol Fe/kg was used considering an improvement in accumulation. In this study, DECT confirmed its accumulation, but the optimal dose may differ between MRI and CT. In the future, the optimal dose for clinical application in humans should be

examined. Previous studies reported USPIO administration to humans (12,14) and we evaluated its accumulation using DECT, which facilitates coronary-artery assessment; therefore, DECT could be clinically applied for noninvasive molecular imaging of coronary inflammation in near future.

This study has several limitations. In the rabbits used in this study, CT was performed under deep anesthesia and respiratory depression was not conducted. Therefore, the appearance of motion artifacts related to respiration may have influenced the study results. Furthermore, plain CT was not performed before CMEADM-U administration, and it was difficult to differentiate CMEADM-U accumulation from calcification in a high-density area in arteriosclerotic lesions based on CT findings alone. However, pathologically, there were correlations between the grade of a high-density area and degree of hemosiderosis on Berlin blue staining or RAM11-positive macrophages. In addition, pathological findings in a high-density area did not always include calcification; therefore, a high-density area could reflect CMEADM-U accumulation.

In conclusion, the macrophage accumulation of CMEADM-U in arteriosclerotic lesions could be evaluated by adopting DECT *in vivo* in a rabbit model od induced aortic atherosclerosis.

References

1. Burke AP, Farb A, Malcom GT, et al. Coronary risk factors and plaque morphology in men with coronary disease who died suddenly. N Engl J Med 1997;336:1276-1282
2. Stary HC, Chandler AB, Dinsmore RE, et al. A definition of advanced types of atherosclerotic lesions and a histological classification of atherosclerosis. A report from the committee on vascular lesions of the council on arteriosclerosis, American heart association. Arteriosclerosis, Thrombosis Vasc Biol 1995;15:1512-1531
3. Narula J, Finn AV, Demaria AN. Picking plaques that pop. J Am Coll Cardiol 2005; 45: 1970-1973
4. Tang TY. Muller KH. Graves MJ. et al. Iron oxide particles for atheroma imaging. Arterioscler Thromb Vasc Biol 2009; 29: 1001-1008
5. Sigovan M. Boussel L. Sulaiman A. et al. Rapid-Clearance Iron Nanoparticles for Inflammation Imaging of Atherosclerotic Plaque: Initial Experience in Animal Model. Radiology. 2009; 252: 401-409
6. K. Tsuchiya, N. Nitta, A. Sonoda, et al. Atherosclerotic imaging using 4 types of superparamagnetic ironoxides: New possibilities for mannan-coated particles, Eur J Radiol 2013; 82: 1919-1925
7. Yu, LF. Leng, S. McCollough, CH. Dual-Energy CT-Based Monochromatic Imaging. American Journal of Roentgenology 2012: 199: S9-S15
8. McCollough CH. Leng SA. Yu LF. et al. Dual- and Multi-Energy CT: Principles, Technical Approaches, and Clinical Applications. Radiology. 2015; 276: 637-653
9. Sato H, Fujimoto S, Kogure Y, et al. Feasibility of Macrophage Plaque Imaging Using Novel Ultrasmall Superparamagnetic Iron Oxide in Dual Energy CT. Eur J Radiol Open. 2018; 5: 87-91
10. Stefan GR. Claire C. Peter V. et al. Magnetic Resonance Imaging of Atherosclerotic Plaque with Ultrasmall Superparamagnetic Particles of Iron Oxide in Hyperlipidemic Rabbit. Circulation. 2001; 103: 415-422
11. Sigovan M. Boussel L. Sulaiman A. et al. Rapid-Clearance Iron Nanoparticles for Inflammation Imaging of Atherosclerotic Plaque: Initial Experience in Animal Model. Radiology 2009;252:401-409.

12. Corot C. Petry KG, Trivedi R, et al. Macrophage Imaging in Central Nervous System and in Carotid Atherosclerotic Plaque Using Ultrasmall Superparamagnetic Iron Oxide in Magnetic Resonance Imaging. Invest Radiol. 2004 ;39: 619-625
13. Kooi ME. Cappendijk VC. Cleutjens KB. et al. Accumulation of ultrasmall superparamagnetic particles of iron oxide in human atherosclerotic plaques can be detected by in vivo magnetic resonance imaging. Circulation. 2003; 19: 2453-2458
14. Schmitz SA. Taupitz M. Wagner S. et al. Magnetic resonance imaging of atherosclerotic plaques using superparamagnetic iron oxide particles. Journal of Magnetic Resonance Imaging 2001;14:355-361.

Figure legends

	grade 0	grade 1	grade 2	grade 3	grade 4
Berlin blue	0	20	4	0	0

Fig 1: Pathological images and dual energy CT images of NZW rabbit with CMEADM-U. (a)hematoxylin & eosin stain image, (b) berlin blue stain image, (c) RAM11 image, (d)70kev image, (e) 35keV image, and (f) iron-based map image in NZW rabbit.

Fig 2: Pathological images and dual energy CT images of WHHL rabbit with CMEADM-U. (a) hematoxylin & eosin stain image, (b) berlin blue stain image, (c) RAM11, (d)70kev image, (e) 35keV image, and (f) iron-based map image, image in WHHL rabbit**.**

Fig 3: Comparison of CMEADM-U intensity with DECT images between grade 1 and 2 at positive areas on berlin blue staining**.** Comparison between the grade 1 and 2 sections; (a) at 70keV image, (b) at 35keV image, and (c) an iron-based map image with berlin blue.

Fig 4: Comparison of CMEADM-U intensity with DECT images between grade 2, 3 and 4 at positive areas on RAM11 immunostaining. Comparison between the grade 2, 3 and 4 sections; (a) at 70keV image, (b) at 35keV image, and (c) iron-based map image with RAM11**.**

Fig 5: Correlation between CMEADM-U intensity with DECT images and positive area with RAM11. Correlation between contrast enhancement (a) at 70keV images, (b) at 35keV images, and (c) an iron-based map images of CMEADM-U and positive area with RAM11 on the corresponding aortic cross-sections.

Table 1: Results of grade classification for positive areas at berlin blue staining and RAM11 immunostaining.

RAM11	0	0	5	8	11

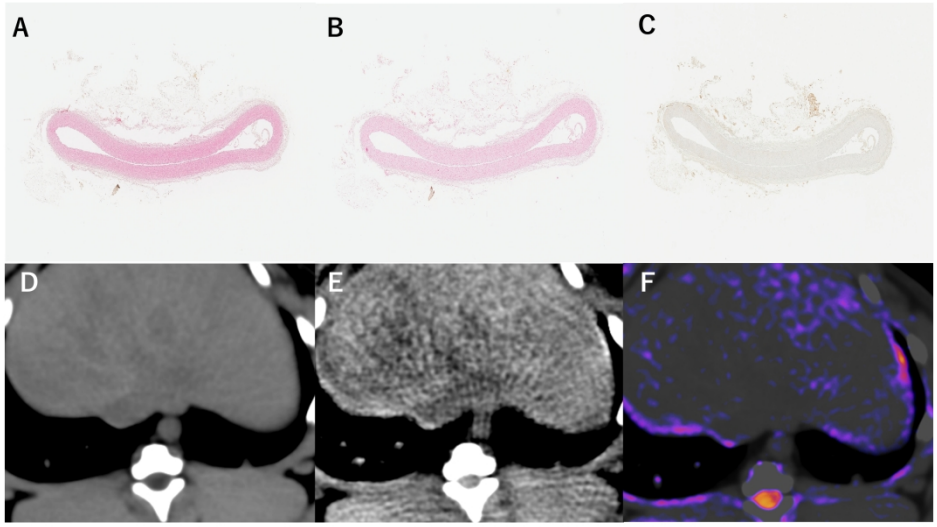

Pathological images and dual energy CT images of NZW rabbit with CMEADM-U
(a)hematoxylin & eosin stain image, (b) berlin blue stain image, (c) RAM11 image, (d)70kev image, (e) 35keV image, and (f) iron-based map image in NZW rabbit.

338x190mm (300 x 300 DPI)

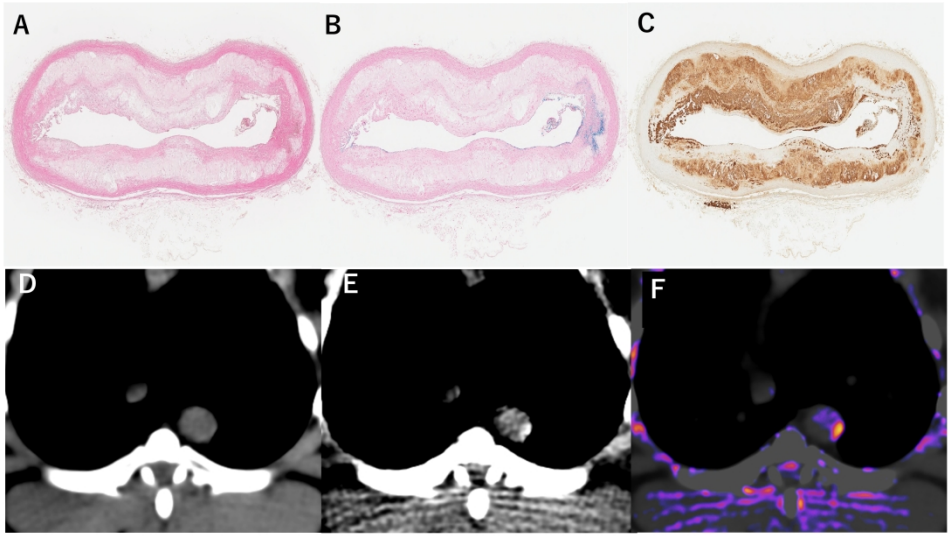

Pathological images and dual energy CT images of WHHL rabbit with CMEADM-U
(a) hematoxylin & eosin stain image, (b) berlin blue stain image, (c) RAM11, (d)70kev image, (e) 35keV image, and (f) iron-based map image, image in WHHL rabbit.

338x190mm (300 x 300 DPI)

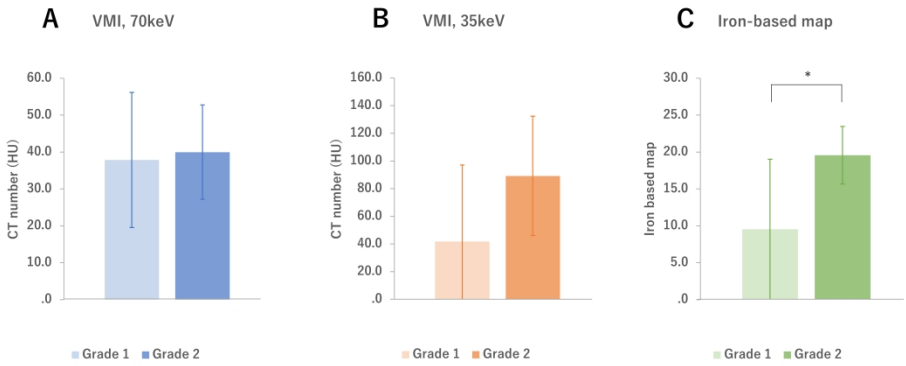

Comparison of CMEADM-U intensity with DECT images between grade 1 and 2 at positive areas on berlin blue staining
Comparison between the grade 1 and 2 sections; (a) at 70keV image, (b) at 35keV image, and (c) an iron-based map image with berlin blue.

338x190mm (300 x 300 DPI)

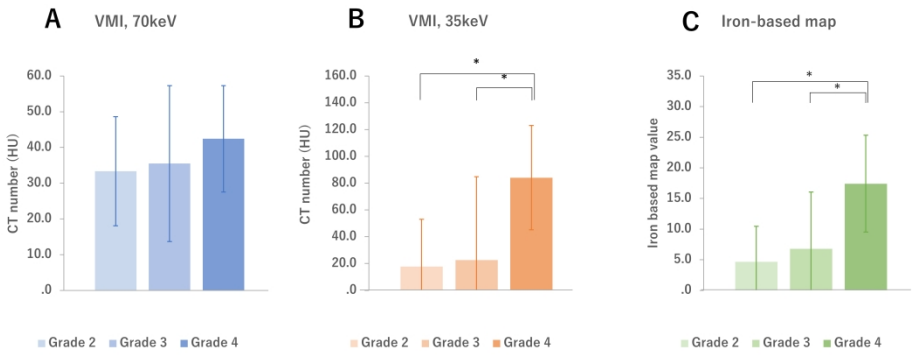

Comparison of CMEADM-U intensity with DECT images between grade 2, 3 and 4 at positive areas on RAM11 immunostaining
Comparison between the grade 2, 3 and 4 sections; (a) at 70keV image, (b) at 35keV image, and (c) iron-based map image with RAM11.

338x190mm (300 x 300 DPI)

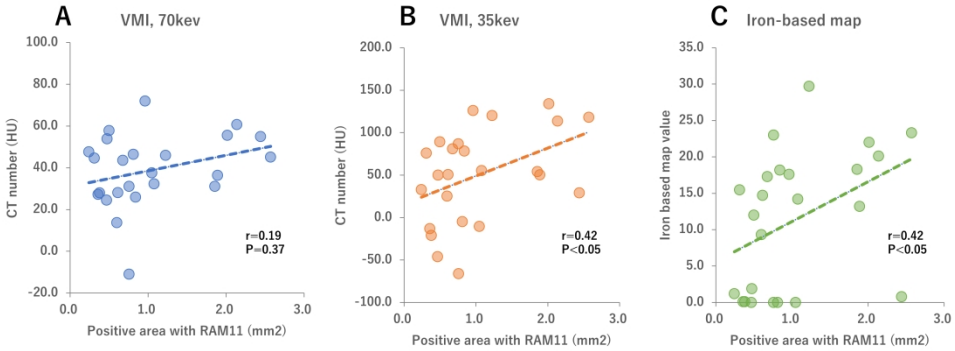

Correlation between CMEADM-U intensity with DECT images and positive area with RAM11
Correlation between contrast enhancement (a) at 70keV images, (b) at 35keV images, and (c) an iron-based map images of CMEADM-U and positive area with RAM11 on the corresponding aortic cross-sections.

338x190mm (300 x 300 DPI)